Pure Appl. Chem., Vol. 74, No. 9, pp. 1545–1552, 2002.

Nanotubes of the disulfides of groups 4 and 5 metals*

Manashi Nath[1] and C. N. R. Rao[2,‡]

[1]Chemistry and Physics of Materials Unit, Jawaharlal Nehru Center for Advanced Scientific Research, Bangalore 560 064, India; [2]Solid State and Structural Chemistry Unit, Indian Institute of Science, Bangalore 560 012, India

Abstract: Nanotubes of HfS_2, ZrS_2, NbS_2, and TaS_2 have been obtained by the reduction of the corresponding metal trisulfides in a stream of H_2 (mixed with an inert gas in some cases) at elevated temperatures. The nanotubes have been characterized by transmission electron microscopy (TEM) and other techniques. These disulfide nanotubes make an important addition to the growing family of nanotubes of inorganic layered materials.

INTRODUCTION

The layered chalcogenides, having structures analogous to graphite, are known to be unstable toward bending and show high propensity to form curved structures, thus eliminating dangling bonds at the edges. Since the discovery of fullerene and nanotube structures of WS_2 and MoS_2 by Tenne et al. [1–3], there have been attempts to prepare and characterize nanotubes of other layered dichalcogenides with structures analogous to MoS_2. Nanotubes of MoS_2 and WS_2 were prepared by Tenne et al. by reducing the corresponding oxides to the suboxides followed by heating in an atmosphere of forming gas (5 % H_2 + 95 % N_2) and H_2S at 700–900 °C [1–3]. Alternative methods of synthesis of MoS_2 and WS_2 nanotubes have since been proposed by employing the decomposition of the ammonium thiometallates or the corresponding trisulfide precursors. This alternative procedure was based on the observation that the trisulfide seems to be formed as an intermediate in the synthesis of the MoS_2 and WS_2 nanotubes [4]. Accordingly, the decomposition of the trisulfides of Mo and W in a reducing atmosphere directly yielded nanotubes of the disulfides MoS_2 and WS_2 [5]. In this article, we describe the synthesis, structure, and characterization of a few novel nanotubes of the disulfides of groups 4 and 5 metals. These include nanotubes of NbS_2, TaS_2, ZrS_2, and HfS_2. The study enlarges the scope of the inorganic nanotubes significantly and promises other interesting possibilities, including the synthesis of the diselenide nanotubes of these metals.

SYNTHESIS AND CHARACTERIZATION

The trisulfides were prepared by the conventional solid-state synthesis route. Powders of the metal and sulfur were mixed in the stoichiometric ratio and heated in evacuated and sealed quartz ampoules to 700, 850, 700, and 560 °C to obtain NbS_3, TaS_3, ZrS_3, and HfS_3, respectively [6–9]. Unlike MoS_3 and WS_3, which are amorphous [4], the trisulfides of the groups 4 and 5 metals are crystalline [9]. In spite of this, the decomposition of the trisulfides in a reducing atmosphere at elevated temperatures produced good yield of nanostructures, including nanorods and nanotubes. The nanostructures have been charac-

Pure Appl. Chem.* **74, 1489–1783 (2002). An issue of reviews and research papers based on lectures presented at the 2nd IUPAC Workshop on Advanced Materials (WAM II), Bangalore, India, 13–16 February 2002, on the theme of nanostructured advanced materials.

‡Corresponding author: E-mail: cnrrao@jncasr.ac.in

terized by TEM, scanning electron microscopy (SEM), powder X-ray diffraction (PXRD), and optical measurements such as Raman and photoluminescence.

HfS_2 nanotubes

The nanotubes of HfS_2 have been prepared by the decomposition of HfS_3 in an atmosphere of H_2 + Ar (1:9), at 900 °C. The product contained a good yield of the nanostructures, as can be seen from the SEM image in Fig. 1a. The EDX analysis revealed the chemical composition to be HfS_2. The XRD pattern confirmed the phase as 1T-HfS_2 having the lattice parameters a = 3.635 and c = 5.851 Å [JCPDS file card no.: 28-0444]. There is a slight expansion in the c-direction (~1 %) for the nanotubes as compared to the bulk HfS_2. The lattice expansion is less than that observed for the MoS_2 and WS_2 nanotubes (2–3 %) [10]. This can be attributed to the fact that the mean compressibility factor of the c-axis in HfS_2 is higher than that observed for MoS_2 [11]. The nanostructures as can be seen from the SEM image in

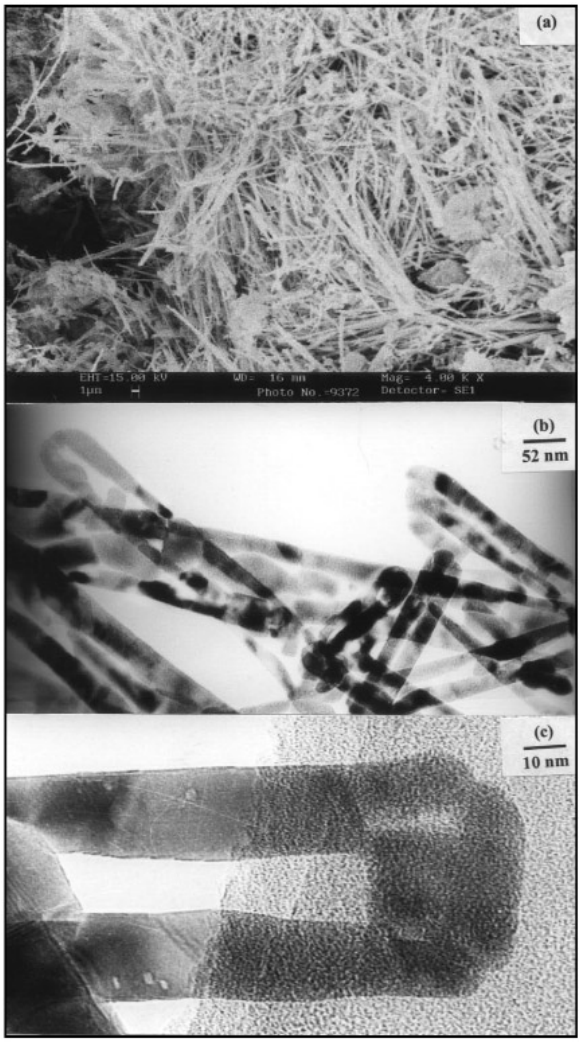

Fig. 1 (a) SEM image of the HfS_2 nanotubes; (b)–(c) low-resolution TEM image of the HfS_2 nanotubes. Some of the tubes show closed rectangular tips.

Fig. 1a are quite lengthy, some being more than a micron long. Interestingly, a large proportion of these nanostructures are nanotubes. A low-resolution TEM image in Fig. 1b shows several nanotubes, some of which are closed with a nonspherical, nearly rectangular tip. The outer diameters of the tubes are in the range of 55–60 nm, while the inner diameter is in the range of 17–30 nm. The image in Fig. 1c shows a single nanotube with a rectangular tip, showing ripple-like undulations near the bend, which can arise from the strain involved in bending the layers. On close inspection, layer fringes are visible along the tube walls. Interrupted layer growth is observed in the inner edge of the tube wall, causing terminated layers and thus nonuniformity in the wall thickness. This type of rectangular tip and terminated layer growth has also been observed in the MoS_2, WS_2, and $Mo_{1-x}W_xS_2$ nanotubes [12,13]. A high-resolution image of the HfS_2 nanotube is shown in Fig. 2. The layers are separated by ~5.8 Å, corresponding to the spacing of the (001) planes. Several terminated layers are observed at the outer edge of the tube wall, possibly owing to the absence of growing materials at these edges. A considerable amount of defects and edge dislocations are also present along the length of the tube wall. The inset shows an ED pattern of the nanotube, characteristic of the hexagonal arrangement of the layers with the spots corresponding to d(002) plane (2.923 Å). The ED pattern, together with the high-resolution image, indicates that the tube growth axis is perpendicular to the *c*-direction.

Bulk HfS_2 is an indirect band-gap semiconductor with an indirect band-gap energy of ~2.1 eV [14]. The reflectance spectrum of the nanotubes shows a small blue shift compared with the bulk. The photoluminescence spectra of the nanotubes show a peak at 676 nm, which is blue-shifted with respect to the peak observed at 687 nm for bulk HfS_2 powder (see Fig. 3a). Raman studies were also performed on the HfS_2 nanotubes. The Raman spectrum of the HfS_2 nanotubes is shown in Fig. 3b. It shows a band due to the A_{1g} mode, corresponding to the S atom vibration along the *c*-axis perpendicular to the basal plane, and another due to the E_g mode due to the movement of the S and Hf atoms in the basal plane [15]. The Raman bands of the nanotube correspond exactly to the bands obtained for the bulk HfS_2 powder, but the A_{1g} band shows some broadening. The full width at half-maximum (fwhm) of the A_{1g} band is 11 cm^{-1} in the nanotubes compared to 8 cm^{-1} for the bulk sample. Such a broadening of the Raman band has also been noted in MoS_2 and WS_2 nanotubes [10].

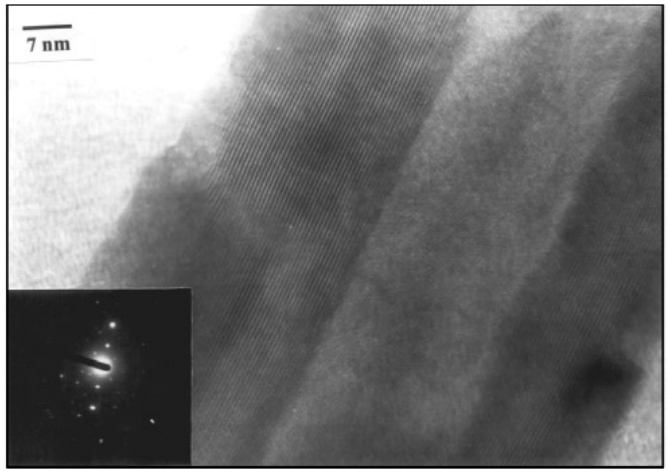

Fig. 2 High-resolution TEM image of the HfS_2 nanotube, showing lattice fringes with a layer separation of ~5.8 Å. The inset shows the ED pattern of the nanotube.

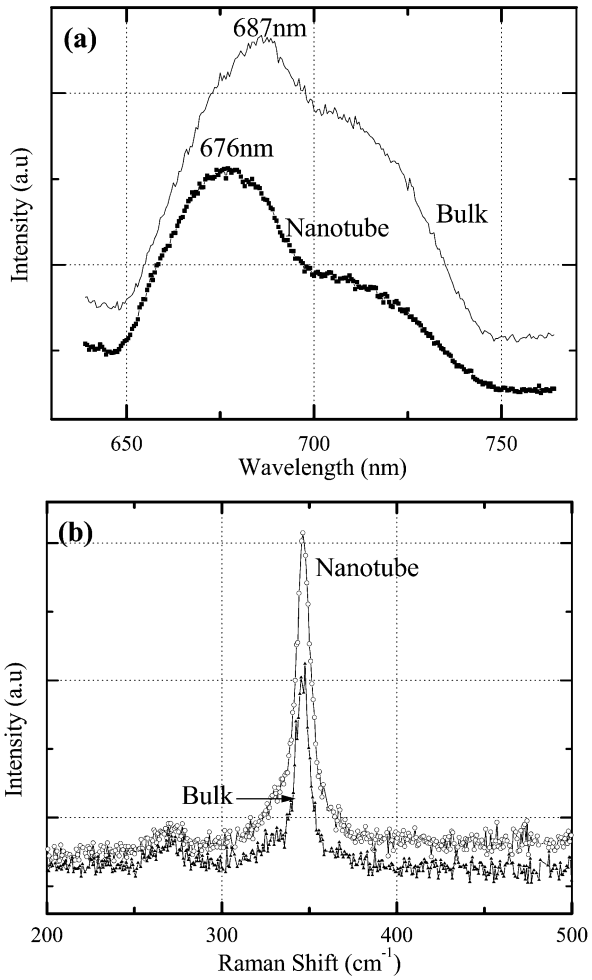

Fig. 3 (a) Photoluminescence spectra of HfS_2 nanotubes and bulk HfS_2; (b) Raman spectra of HfS_2 nanotubes and HfS_2 bulk.

ZrS_2 nanotubes

ZrS_2 nanotubes could be similarly prepared by the thermal decomposition of ZrS_3 under H_2 + Ar at 900 °C. The EDX analysis coupled with the XRD pattern of the products confirmed the product to be hexagonal ZrS_2 having lattice parameters of with a = 3.660 Å and c = 5.825 Å [JCPDS card no.: 11-0679]. The low-resolution image in Fig. 4a shows a closed ZrS_2 nanotube having a rectangular tip. The outer diameter of the nanotube is ~125 nm while the inner core diameter is ~60 nm. Besides nanotubes, other structures such as nanorods and nano-onions are also seen in the image. Figure 4b shows the TEM image of a single ZrS_2 nanotube having a rectangular tip with undulations in the outer edge similar to those observed for HfS_2 tubes. The inner wall of the tube shows nonuniformity near the tip resulting from the discontinuous growth of the ZrS_2 layers. The inset shows an ED pattern of the ZrS_2 tube with characteristic hexagonal arrangement of the spots corresponding to d(002).

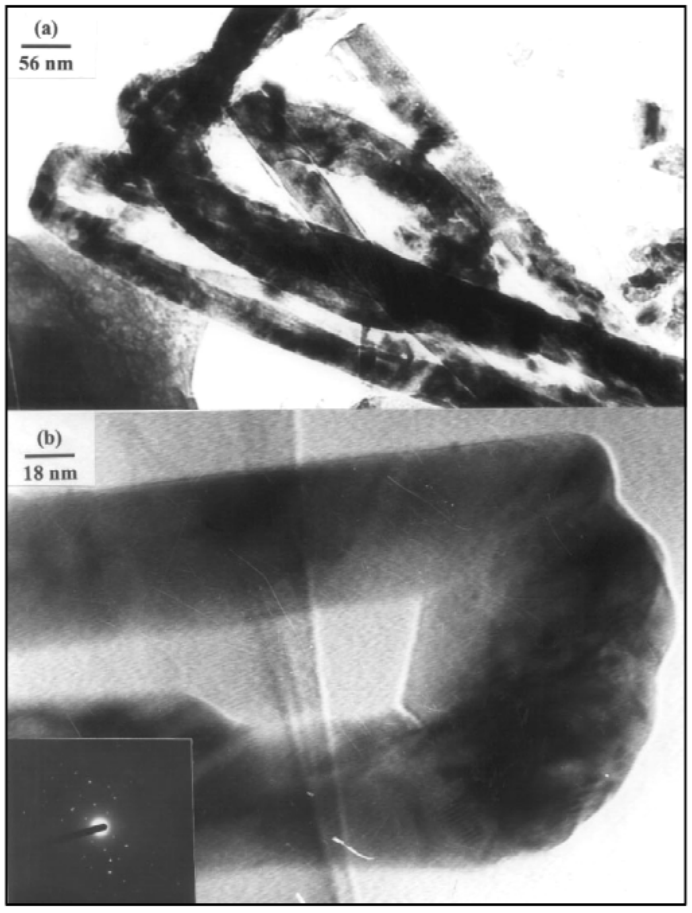

Fig. 4 (a) Low-resolution TEM image of ZrS_2 nanostructures showing nanorods and onions besides nanotubes; (b) TEM image of a single nanotube showing a rectangular cap.

NbS_2 nanotubes

NbS_3 when heated in a stream of H_2 (100 sccm) at 1000 °C for 30–60 min, produces good yield of nanostructures [16]. EDX analysis and XRD pattern of the product confirmed the formation of 2H-NbS_2. A *c*-axis expansion of ~3 % has been observed in the nanotubes. The SEM image in Fig. 5a shows the high yield of the nanostructures obtained by the thermal decomposition of the trisulfide under H_2. These nanostructures contained a considerable amount of nanotubes, as can be seen from the TEM images. The TEM image in Fig. 5b shows couple of nanotubes, having closed rectangular tips. The diameters of the hollow tubules are in the range ~4–15 nm. Interestingly, while some of the nanotubes are closed with flat nonspherical polygonal tips, most of the tubes are observed to be open in one or both the ends. The image in Fig. 5c shows the high-resolution image of an open nanotube. The layer separation in the walls is ~6 Å, corresponding to the (002) plane of bulk NbS_2 [JCPDS file card no.: 41-0980]. The ED pattern in the inset shows the nanotube to be single-crystalline with Bragg spots corresponding to the known *d* values. Some of the diffraction spots show diffuse scattering or streaking owing to bent layers or disorder.

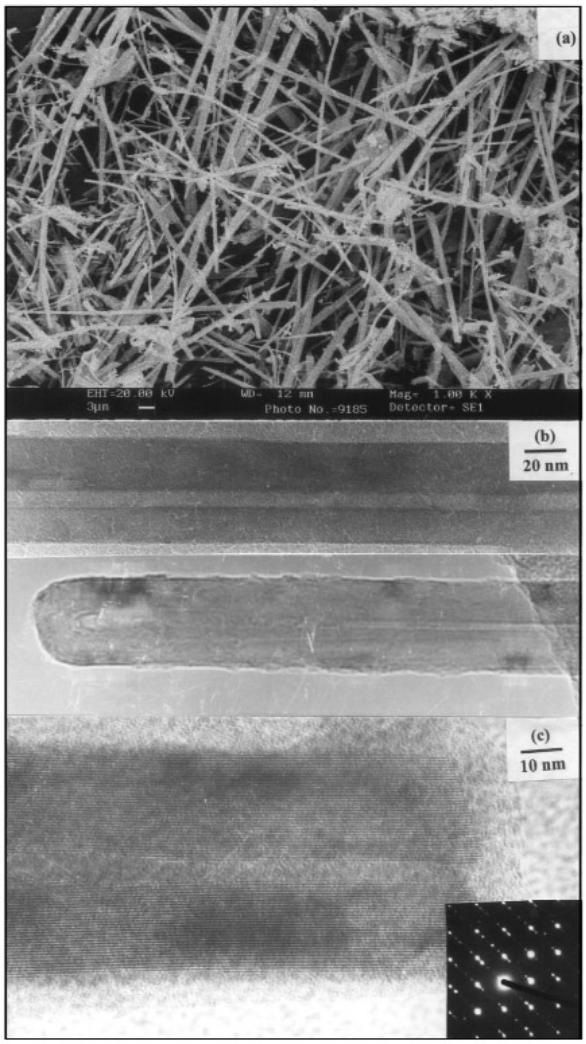

Fig. 5 (a) SEM image of the NbS_2 nanostructures showing a good yield; (b) low-resolution image of the NbS_2 nanotubes, showing nonspherical cap; (c) high-resolution TEM image of the NbS_2 nanotube showing a layer spacing of ~6 Å. The inset shows a typical ED of the NbS_2 nanotube.

TaS_2 nanotubes

The TaS_2 nanotubes were prepared by decomposing TaS_3 at 1000 °C under H_2 (100 sccm). The SEM image in Fig. 6a reveals that a good yield of the nanostructures is obtained. The EDX analysis and the XRD confirmed the product as 2H-TaS_2. TEM observation of the product showed the presence of hollow-core nanotubes in the product. The low-resolution image in Fig. 6b shows a TaS_2 nanotube having a diameter of ~30 nm. The inner wall shows nonuniformity along the length of the tube. Some of the tubes are closed with flat rectangular tips, as can be seen from the image in Fig. 6c. The inset shows a typical ED pattern of the nanotubes, revealing Bragg spots with *d* values in agreement with the literature [JCPDS file card no.: 02-0137].

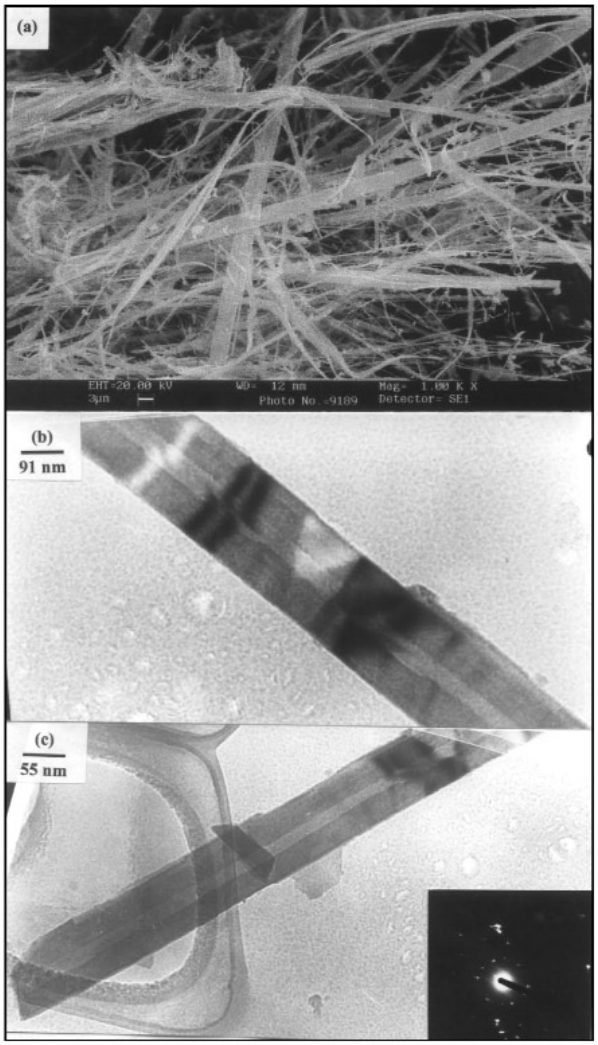

Fig. 6 (a) SEM image of the TaS_2 nanostructures; (b)–(c) low-resolution TEM images of the TaS_2 nanotubes. The tube in (c) exhibits a flat rectangular tip. The inset shows a typical ED pattern.

MECHANISM OF GROWTH

The trisulfide particles decompose to form the disulfides by the simple reaction,

$$MS_3\ (+\ H_2) \longrightarrow MS_2 + S\ (H_2S)$$

The trisulfide precursor particles are slowly heated above their corresponding decomposition temperatures to initiate tube growth. Under gas flow, the precursor particles may be reduced to the nanoparticulate form, which act as nuclei for the tube growth. Initially, a few of the disulfide layers are formed at the outer edge of the precursor particles, which entrap the particle and inhibit two such particles to form larger aggregates. Further decomposition gives rise to growing disulfide layers, which protrude outwards. Thus, the growth proceeds outwards from the core of the particles. This type of "inside-out" growth is facilitated by defects, edge dislocations, and terminated layers near the tip and the tube walls, which are the active points of tube growth (see Figs. 1b, 1c, 2b). Absence of the trisulfide particles

inside any disulfide tubes indicates the growth mechanism to be different from the catalyst-mediated growth process of the carbon nanotubes, where the nanotubes contain metal particle inside the tube. In the case of carbon nanotubes, diffusion of carbon into the metal catalyst particle makes the graphene sheets grow out from the rear end of the particle, thereby often engulfing the catalyst particle inside the tube. In the case of the disulfide tubes, the tube tips generally contain defects and dislocations, and, in some cases, domains containing a few layers of the starting trisulfide can also be identified. Clearly, the tip region is the active region for the tube growth.

CONCLUSIONS

The present study shows that the reduction of crystalline trisulfides of groups 4 and 5 metals in an atmosphere of Ar and H_2 around 900–1000 ºC gives rise to the nanotubes of the corresponding disulfides. Clearly, the trisulfide route provides a useful means of generating such nanostructures. The nanotubes have quite large diameters, and it may be possible to control the diameter by varying the reaction conditions. The nanotubes generally show the presence of organized layers of the disulfide along the tube walls. Unusual tip structures are also encountered besides defects and terminated layers.

REFERENCES

1. R. Tenne, L. Margulis, M. Genut, G. Hodes. *Nature* **360**, 444 (1992).
2. L. Margulis, G. Salitra, M. Taliankar, R. Tenne. *Nature* **365**, 113 (1993).
3. Y. Feldman, E. Wasserman, D. J. Srolovitch, R. Tenne. *Science* **267**, 222 (1995).
4. G. U. Kulkarni and C. N. R. Rao. *Catal. Lett*. **11**, 63 (1991).
5. M. Nath, A. Govindaraj, C. N. R. Rao. *Adv. Mat*. **13**, 283 (2001).
6. N. Allali, V. Gaborit, E. Prouzet, C. Geantet, M. Danot, A. Nadiri. *J. Phys. IV* **7**, 927 (1997).
7. E. Bjerkelund and A. Kjekshus. *Z. Anorg. Allg. Chemie* **328**, 235 (1964).
8. Mc. Taggart and A. D. Wadsley. *Aust. J. Chem.* **11**, 445 (1958).
9. C. N. R. Rao and K. P. R. Pisharody. *Progr. Solid State Chem.* **10**, 207 (1975).
10. G. L. Frey, R. Tenne M. J. Matthews, M. S. Dresselhaus, G. Dresselhaus. *J. Mater. Res.* **13**, 2412 (1998).
11. H. D. Falck. *J. Appl. Cryst.* **5**, 138 (1972).
12. Y. Q. Zhu, W. K. Hsu, H. Terrones, N. Grobert, B. H. Chang, M. Terrones, B. Q. Wei, H. W. Kroto, D. R. M. Walton, C. B. Boothroyd, I. Kinloch, G. Z. Chen, A. H. Windle, D. J. Fray. *J. Mater. Chem*. **10**, 2570 (2000).
13. M. Nath, K. Mukhopadhyay, C. N. R. Rao. *Chem. Phys. Lett.* **352**, 163 (2002).
14. D. L. Greenaway and R. Nitsche. *J. Phys. Chem. Solids* **26**, 1445 (1965).
15. M. I. Nathan, M. W. Shafer, J. E. Smith. *Bull. Am. Phys. Soc.* **17**, 336 (1972).
16. M. Nath and C. N. R Rao. *J. Am. Chem. Soc.* **123**, 4841 (2001).